UC San Diego

UC San Diego Previously Published Works

Title

Tuning Oxygen Redox Reaction through the Inductive Effect with Proton Insertion in Li-Rich Oxides.

Permalink

https://escholarship.org/uc/item/4wm4v0kf

Journal

ACS applied materials & interfaces, 12(6)

ISSN

1944-8244

Authors

Wu, Jue
Zhang, Xiaofeng
Zheng, Shiyao
et al.

Publication Date

2020-02-01

DOI

10.1021/acsami.9b21738

Peer reviewed

eScholarship.org Powered by the California Digital Library
University of California

Tuning Oxygen Redox Reaction Through Inductive Effect with Proton Insertion in Li-rich Oxides

Jue Wu[1,2], Xiaofeng Zhang[3], Shiyao Zheng[1], Haodong Liu[4], Jinpeng Wu[2], Riqiang Fu[5], Yixiao Li[1], Yuxuan Xiang[1], Rui Liu[1], Wenhua Zuo[1], Zehao Cui[1], Qihui Wu[6], Shunqing Wu[3], Zonghai Chen[7], Ping Liu[4], Wanli Yang[2], Yong Yang[1]**

[1] State Key Laboratory for Physical Chemistry of Solid Surfaces, Collaborative Innovation Center of Chemistry for Energy Materials, Department of Chemistry, College of Chemistry and Chemical Engineering, and College of Energy, Xiamen University, Xiamen 361005, China.

[2] Advanced Light Source, Lawrence Berkeley National Laboratory, One Cyclotron Road, Berkeley, California 94720, USA.

[3] Department of Physics, Collaborative Innovation Center for Optoelectronic Semiconductors and Efficient Devices, Key Laboratory of Low Dimensional Condensed Matter Physics (Department of Education of Fujian Province), and Jiujiang Research Institute, Xiamen University, Xiamen 361005, China.

[4] Department of NanoEngineering, University of California San Diego, La Jolla, California 92093, USA.

[5] National High Magnetic Field Laboratory, Florida State University, 1800 E. Paul Dirac Drive, Tallahassee, Florida 32310, USA.

[6] Department of Materials Chemistry, School of Chemical Engineering of Materials Science, Quanzhou Normal University, Quanzhou 362000, China.

[7] Chemical Sciences and Engineering Division, Argonne National Laboratory, Lemont, Illinois 60439, USA.

Corresponding Author

* yyang@xmu.edu.cn

* wlyang@lbl.gov

KEYWORDS: High capacity battery, ~~cathode~~Oxygen redox reaction, ~~high capacity, oxygen activity, p~~Proton insertion, Li-rich oxides cathode, Resonant Inelastic X-ray Scattering (RIXS).

ABSTRACT: As a parent compound of Li-rich electrodes, Li_2MnO_3 exhibits high capacity during the initial charge, however, suffers notoriously low Coulombic efficiency due to ~~irreversible~~ oxygen ~~oxidation~~ and ~~its associated~~ surface activities~~reactions~~. Here, we successfully optimize ~~tune~~ the oxygen activities~~oxidation process~~ towards reversible oxygen redox reactions by intentionally introducing protons into lithium octahedral vacancies in Li_2MnO_3 system with its original structural integrity maintained. Combining structural probes, theoretical calculations and resonant inelastic X-ray scattering results, a moderate coupling between the introduced protons and lattice oxygen at the oxidized state is revealed, which stabilizes the oxygen activities ~~in initial~~during ~~charge~~charging. Such a coupling leads to an unprecedented initial Coulombic efficiency (99.2%) with a ~~further~~ greatly improved discharge capacity of 302 mAh g^{-1} in the protonated Li_2MnO_3 electrodes. These findings directly demonstrate an effective concept for controlling oxygen activities in Li-rich ~~cathodes~~systems, which is critical for developing high-~~capacity~~ energy cathodes in batteries.

TOC GRAPHICS

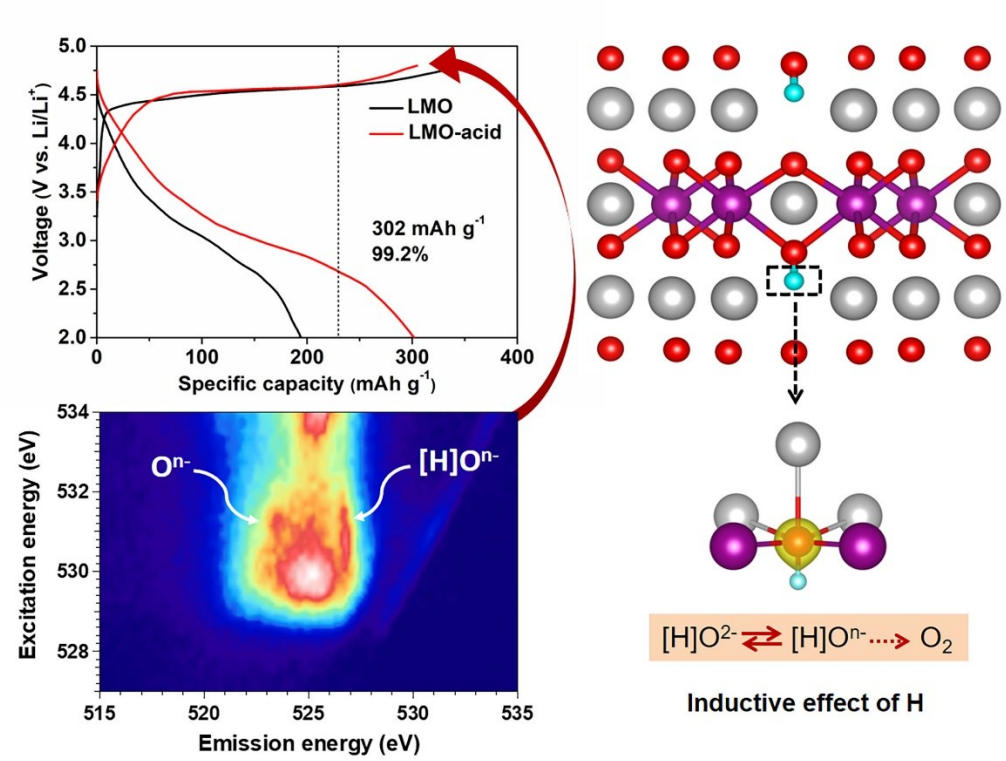

INTRODUCTION

The Li-rich transition metal (TM) oxides have received extensive attention in the past years due to their very high specific capacity of more than 280 mAh g^{-1}[1,2,3]. In general, the improvement of Li-rich materials is based on one of the parent compounds, Li_2MnO_3 (LMO), which contributes to the excessive Li for the improved capacity. However, the practical employment of the extra capacity of Li-rich compounds has so far been hindered by various detrimental effects triggered by the high-capacity cycling, leading to a notoriously low Coulombic efficiency during the initial cycle of LMO[4,5,6,7,8], as well as other practical issues like the voltage decay[9,10,11]. Indeed, it has been reported that the practical issue of voltage decay in Li-rich compounds is

associated with the oxygen activity[12,13,14]. The oxygen release ~~displays~~ is also associated with a significantly low discharge capacity right after the initial charging due to the irreversible oxygen oxidation reactions at high potentials[7,15,16]. Other than this initial cycle reversibility issue, it has been accepted now that the critical challenge for improving the cycling capacity of Li-rich compounds is to control the oxygen oxidation process during the high-capacity charging so reversible reactions could be realized. While it seems indeed possible to have highly reversible oxygen redox reactions in low-cost *3d* TM oxide materials[17], such a challenge for Li-rich material remains. The LMO sample provides an excellent model compounds for exploring the methods on controlling the oxygen activities. Therefore, new strategies and solutions are urgently needed to effectively control the oxygen oxidation process towards a reversible oxygen redox reaction without sacrificing the accessible capacity in *3d* TM electrode systems.

As a matter of fact, it has long been known that the oxygen could be stabilized through the so-called “inductive effect” in olivine-structured $LiFePO_4$, where phosphor is introduced to the vicinity of oxygen and stabilize the oxygen involvements in electrochemistry[18,19,20]. Therefore, if electrochemically inactive positive ions could be introduced and coupled with oxidized oxygen, an inductive effect could hopefully stabilize the severe oxygen oxidation process. In this work, we successfully demonstrated that the intercalated protons into LMO layered materials could stabilize the

oxygen oxidation activities towards reversible oxygen redox, leading to unprecedented Coulombic efficiency with ~~further~~ much improved discharge capacity of LMO electrodes. Note that proton is electrochemically inactive with small ionic radii (r (H^+) ≈ 0.85 fm[21], r (Li^+) = 0.76 Å). Previous works indicate that the Li^+-H^+ exchange takes place on Li-rich cathodes[22,23,24,25]; however, the intrinsic mechanism of protonation effect on the electrochemical properties and especially on the oxygen redox activities has not been explored ~~clearly~~ before. Here, we have employed the structural verifications through X-ray and neutron diffraction experiments to probe the location of proton in LMO prepared by mild solution treatments. More importantly, mapping of resonant inelastic X-ray scattering (mRIXS) experiments and calculation data reveal directly that the oxidized oxygen interacts with the introduced protons, providing an effective inductive effect to maintain the oxygen redox activities towards high discharge capacity in protonated LMO.

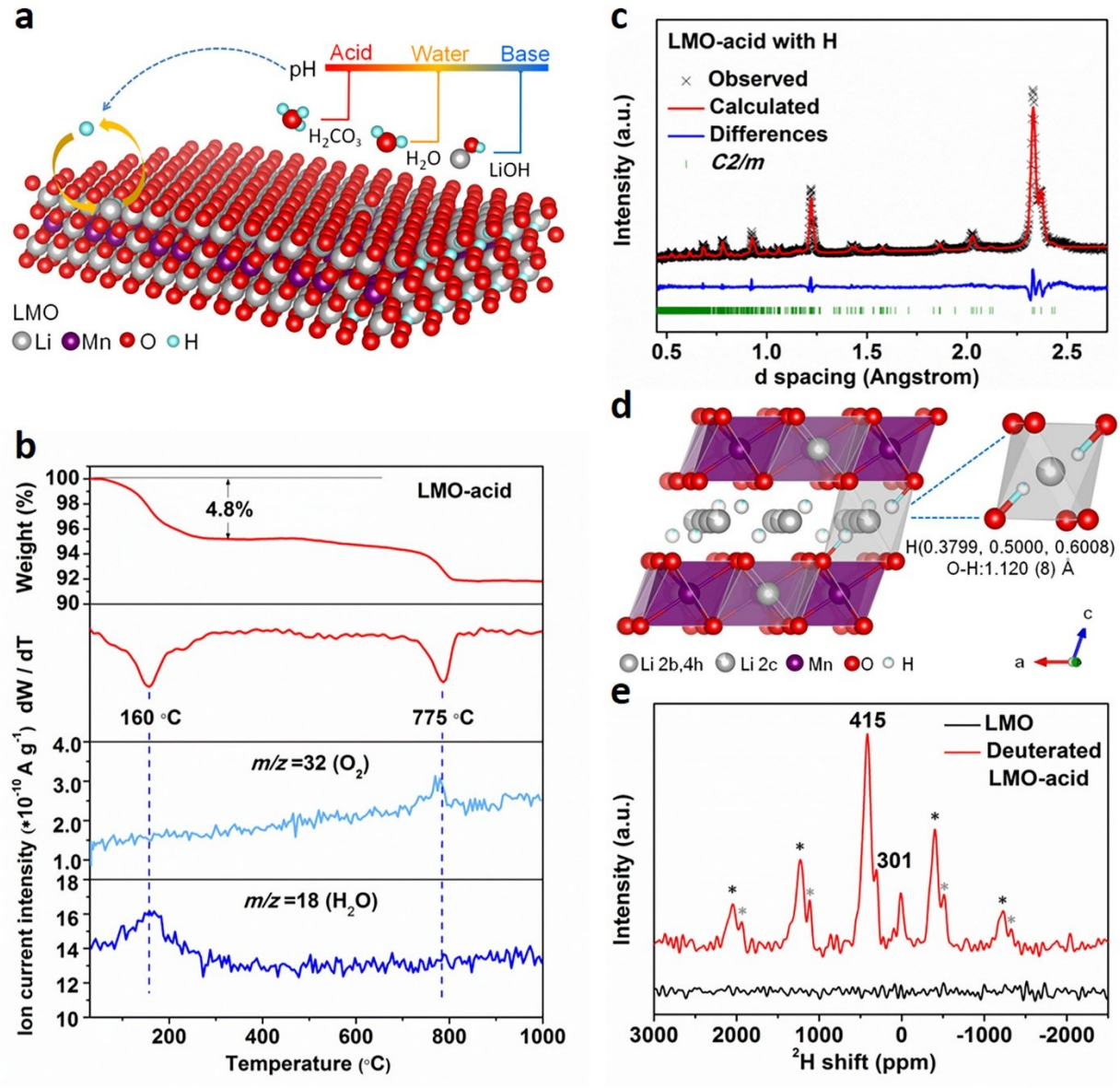

Figure 1. Characterization of protons for pristine and solution-treated LMO. (a) Schematic of solution-treating process for pristine LMO and solutions with different pH values. **(b)** TGA-MS data for LMO-acid sample. **(c)** Rietveld refinement of the normalized ND patterns with protons for LMO-acid sample. **(d)** Schematic representation of protons sites from the refinement of ND patterns. **(e)** ^{2}H NMR spectra for LMO and deuterated LMO-

acid samples. The primary peak at ~415 ppm for deuterated LMO-acid sample is due to ^{2}H insertion into the structure. ∗ indicates sidebands.

Table 1. Chemical analysis data for the solution-treated $Li_{2-x}H_xMnO_3$ samples.

Sample	pH[1]	x[2]	x[3]	Li/Mn[4]
LMO	--	--	--	2.04
LMO-acid	~4.0	0.48	0.47	1.50
LMO-	~7.0	0.23	0.24	1.80
LMO-base	~12.0	0.21	0.20	1.83

(1 for the treating solution; 2 from elemental analysis data; 3 from TGA-MS data; 4 from ICP-AES data; the x value has been corrected with pristine LMO sample to remove the effect of surface water.)

In experimental, the pristine LMO was prepared by a conventional solid-state method (see the 'Method' section). The solution-treating process is schematically shown in **Figure 1**a, where pristine LMO material was treated by solutions with different pH values under mild conditions (**Table S1**). The layered structure with space group of *C2/m* and general morphology are well remained in the treated samples (**Figure S1, Figure S2**). Since pH value of the solution is the only variable in the solution-treating process, it is suspected that the content of protons in different samples may vary. The stoichiometry of Li and Mn was examined by inductively coupled plasma-atomic emission spectrometry (ICP-AES) and shows strong dependence on the pH values of the solutions (**Table 1**). The proton content was then

determined by thermal gravity analysis-mass spectrometry (TGA-MS) measurement (**Figure S3, S4, S5**). For the solution-treated sample, a 18 *m/z* peak is detected at around 160 ℃ (**Figure 1**b), corresponding to the removal of water molecules from the combination of lattice protons and oxygen in sample[24,26,27,28].

The occupancy and location of protons in the crystal structure were investigated by neutron diffraction (ND), which possesses high sensitivity for detecting low-atomic-weight elements, such as Li, H[29,30,31] and D[23]. The refinement was performed with starting model of LMO[32] with proton (**Figure 1**c). By combining the results from density functional theory (DFT) calculation (**Figure S6**, **Table S2**) and bond valence sum (BVS) maps (**Figure S7**, **Note S1**), the protons are located in Li octahedral vacancies of the Li layers, moving off center toward the oxygen atoms with an O-H distance of 1.120 (8) Å (as illustrated in **Figure 1**d). The refinement is improved with the decrease of R_{wp} value (**Table S3, Table S4**) for LMO-acid sample, which supports the existence of protons in the interstitial sites. The content of protons yielded from ND refinement is in the same trend with that of TGA-MS and elemental analysis. The discrepancy of the proton amount from different methods may come from the differences in sensitivities and probe area for protons.

The insertion of protons can be further observed by using solid-state nuclear magnetic resonance (ssNMR) spectroscopy (**Figure 1**e). Compared

with the pristine LMO which shows no ^{2}H signals, the acid-treated sample displays a dominant isotropic resonance at 415 ppm. According to previous reports[23,33,34], a large shift of resonance can be a result of the hyperfine interaction between protons and its adjacent Mn ions, through the intervening oxygen anions. Thus, the peak at 415 ppm is assigned to protons inserted inside the bulk lattice. A minor peak at 301 ppm may come from protons in different locations (**Figure S8**), which is consistent with ND result. The peak at around 7 ppm may come from surface absorption[33,34].

Therefore, the combined experiments based on TGA-MS, ssNMR and ND consistently confirm that protons are inserted into the LMO layered structure via the Li^{+}-H^{+} exchange process to form LMO-acid through the solution-treating **(Table 1)**. It is also important to note that, the O-H distance in treated sample (1.12 Å) is much longer than the typical bond length in OH^{-} systems (<1 Å). This indicates that the intercalated H^{+} does not really bond to O and form OH^{-} group.

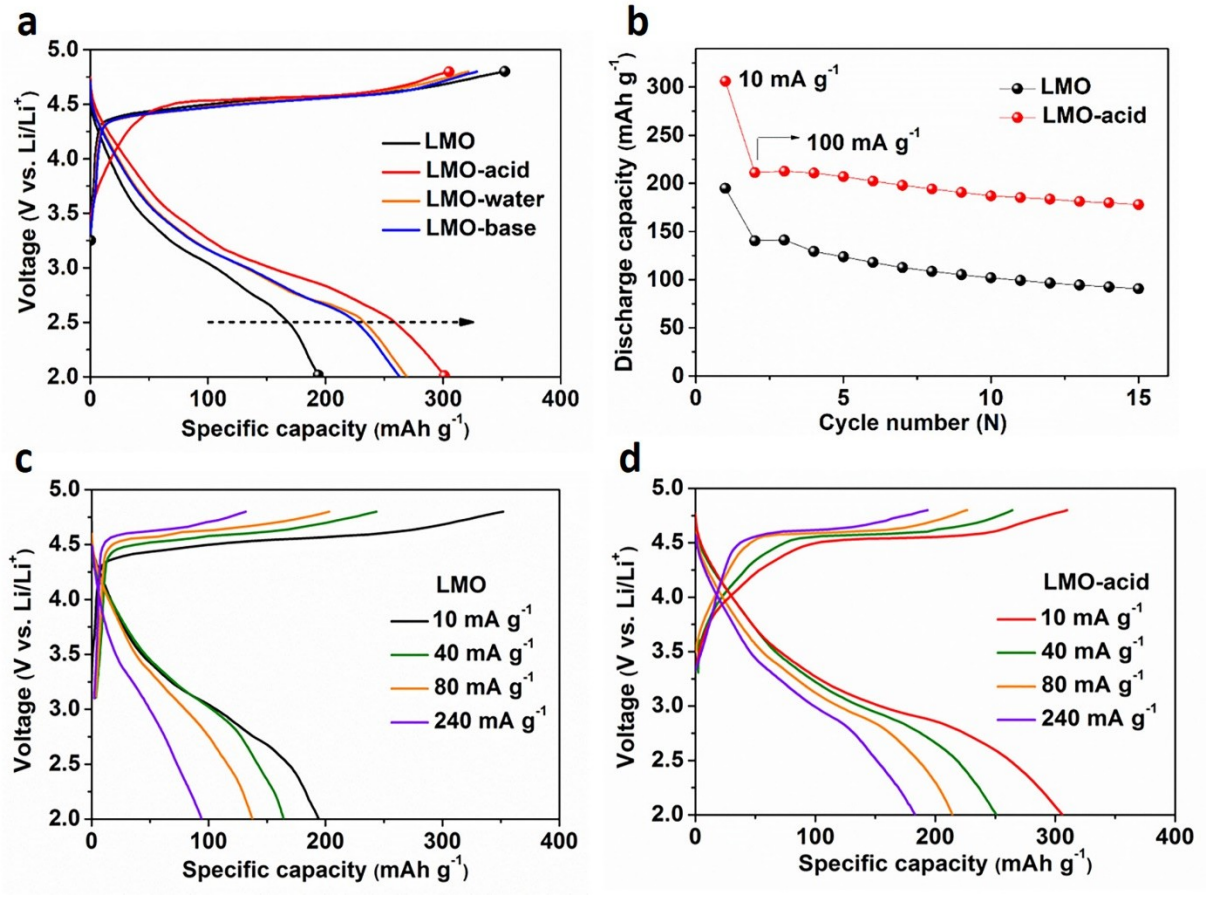

Figure 2. Electrochemical properties of pristine and solution-treated LMO. (a) The initial charge-discharge voltage profiles of pristine and solution-treated LMO samples obtained from Li-half cells at current density of 10 mA g^{-1}. **(b)** Cycling performance of the pristine and LMO-acid samples when cycled at 10 mA g^{-1} in the initial cycle and 100 mA g^{-1} in extended cycles. **(c) (d)** The initial charge-discharge voltage profiles of LMO and LMO-acid samples at different current densities.

The initial cycle voltage profiles of the pristine LMO and solution-treated samples are compared in **Figure 2**a, **Figure S9** and **Table S5**. All samples

exhibit a long plateau region at ~4.5 V versus Li/Li^+, which is mainly ascribed to the removal of Li^+ and oxidation of oxygen anion[35, 16, 36]. Compared with LMO, the initial discharge capacity of LMO-acid is as high as 302 mAh g^{-1} with a Coulombic efficiency of 99.2%, which is superior compared with various optimizations of LMO systems in previous reports. In the first fifteen cycles, LMO-acid sample exhibits a higher discharge capacity (**Figure 2**b). **The conventional LMO exists extremely poor cycling[33], which** is associated with ~~can be affected by~~ **many aspects, such as $Mn^{3+/4+}$ redox participation, Mn dissolution, surface interaction**s**, structural evolution**s **and so on[7, 37,38].** As elaborated below, ~~Since~~ since protonation improves ~~we~~ **only** ~~tune~~ **the oxygen** ~~redox~~ **activity** ~~in this work~~**,** ~~it is reasonable that the enhancement on~~capacity decay ~~cycling is not as~~ remains **obvious** upon extensive cycles ~~as that in the initial cycle~~ in LMO-acid system. Further improvements could be gained through other modifications such as surface coating and/or doping, which is out of the scope of this work. Besides, LMO-acid delivers greatly improved rate capability (**Figure 2**c, **Figure 2**d). Meanwhile, the LMO material was also synthesized at a higher temperature (750 ℃) with no impure phase, which shows similar electrochemical performance in the initial cycle after acid treatment (**Figure S9**).

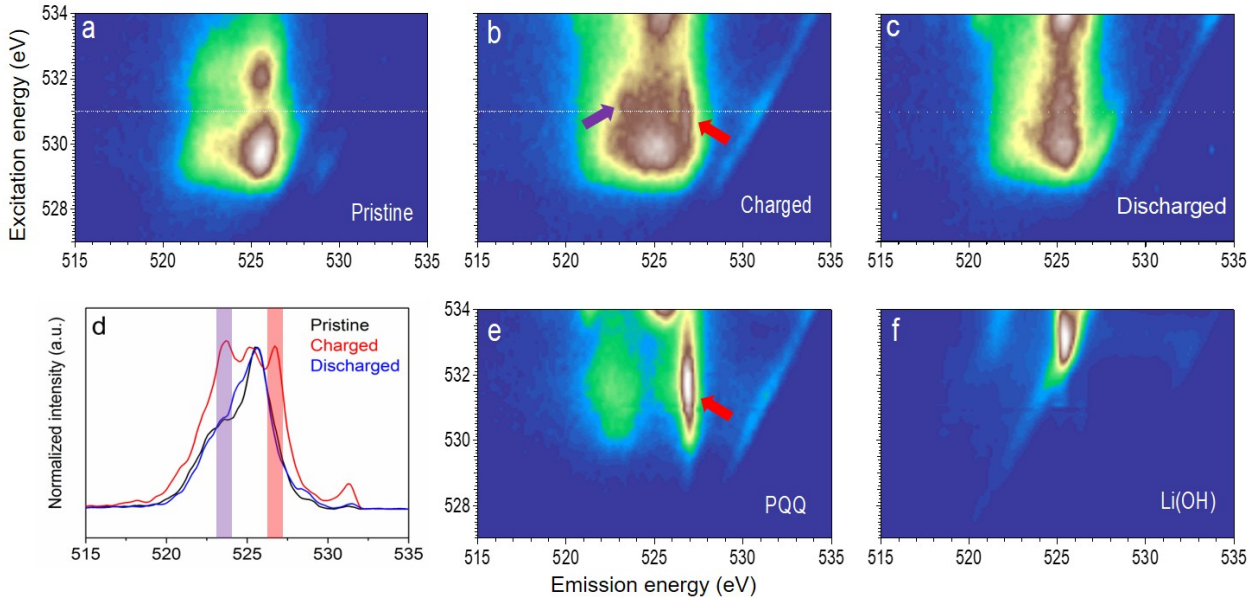

Figure 3. Electronic structures of O probed by mRIXS. (a)(b)(c) The mapping and **(d)** single energy (excitation energy of 531 eV) of O *K*-edge mRIXS spectra for LMO-acid with different electrochemical states, the pristine, 4.8 V charged and 2.0 V discharged, respectively. The intensities in **(d)** are normalized after subtracting the background intensity. The striking oxidized oxygen (purple arrow) and O-H bounding (red arrow) signals are observed in 4.8 V charged LMO-acid. **(e)(f)** The mapping of O *K*-edge mRIXS spectra for PQQ and Li(OH) references.

As introduced above, one of the electrochemical issues in LMO is the large initial irreversibility associated with the irreversible oxygen oxidation. The unprecedented improvement of the discharge capacity in LMO-acid indicates an important effect of proton that could stabilize the oxygen activities. Therefore, we provide a comprehensive study of the mechanism of

protonation effect on oxygen redox through. mRIXS[42], which is has become a tool-of-choice for studying the bulk oxygen redox reactions[39,40,41]. **Figure 3** displays the O *K*-edge mRIXS results on oxygen activities in LMO-acid series samples[17,42,39,40,41]. Strikingly, two features emerge in the 4.8 V charged LMO-acid electrode (**Figure 3**b). One is the known feature at 523.7 eV emission energy (purple arrow), which indicates lattice oxygen is oxidized into reversible oxidized oxygen during charging[39,40,41]. The evolution could be clearly seen in the RIXS cuts shown in **Figure 3**d. In contrast, the pristine LMO series without protons insertion does not display such a reversible behavior of the samee oxidized oxygen features (**Figure S10**), which meaning and analysis is not a topic of this work. Upon discharge, this oxygen feature fades out, indicating a reversible oxygen reduction reaction. The significantly improved Coulombic efficiency and the reversible evolution of the oxidized oxygen mRIXS feature in our protonated LMO-acid directly confirms that the lattice oxygen redox is largely reversible in LMO-acid.

Another strong feature (red arrow in **Figure 3**b) has not been seen reported beforein other oxygen redox systems[17,43,39,40], thus which could beis thus critical for understanding the protonation effect. We therefore investigated the origin of this new feature through comparison with several the reference compounds. It is worth noting that, as elaborated below, such a feature is associated with specific chemical bonding state that may exit in some organic species such as glue or binder, we therefore have tested the

results of the electrodes at different electrochemical states more than once by different experimentalists to make sure that the systematic evolution of this feature is intrinsic and consistently show up in our LMO-acid samples only at the charged state. –**Figure 3**e and **3**f display the mRIXS results collected from pyrroloquinoline quinone (PQQ) and Li(OH) reference samples. The selection of these two sets of references is inspired by their very different O-H bounding: PQQ is a known redox cofactor in biological systems with H^+ only moderately bonded to the oxygen. Actually quinone based materials have recently been reported to be good battery electrodes with H^+ and other alkali ions reversibly bound and unbound from oxygen, again indicating a moderate bonding of H^+ to the oxygen[44,45]. On the contrary, the O-H in Li(OH) is a well formed $(OH)^-$ group with strong bounding that is hard to break.~~, which have different O-H bounding. PQQ is a quinone based material with H^+ only moderately bonded to the oxygen[44,45]. On the contrary, the O-H in Li(OH) is a strong bounding that is hard to break.~~ The mRIXS result of PQQ (**Figure 3e**) displays the clear signature of the moderate O-H bounding configuration at exactly the same emission energy of 527 eV as that of the feature in our protonated LMO electrode (red arrows in **Figure 6b,e**). In sharp contrast, such a feature is completely missing in the Li(OH) sample (**Figure 6f**) with all signals at relatively much higher excitation energies (vertical axis). ~~The mRIXS data comparison between the three samples~~Therefore, the comparison between the LMO-acid electrode and the PQQ/Li(OH) references provides a direct evidence that the protons

introduced into LMO-acid is only moderately coupled to the oxygen, which is consistent with the calculation and ND results. The observation that such a feature is strong in ~~only~~ charged electrodes indicates that i) the intercalated protons are not extracted in the charged state; ii) more importantly, ~~–~~the interaction between protons and oxygen gets enhanced in the oxidized states, which is exactly the state that needs the stabilization of the oxidized oxygen. Such a spontaneous enhancement of O-H bounding in the charged state naturally stabilizes the oxidized oxygen through the inductive effect that has long been known in other battery electrodes like $LiFePO_4$[18,19,20].

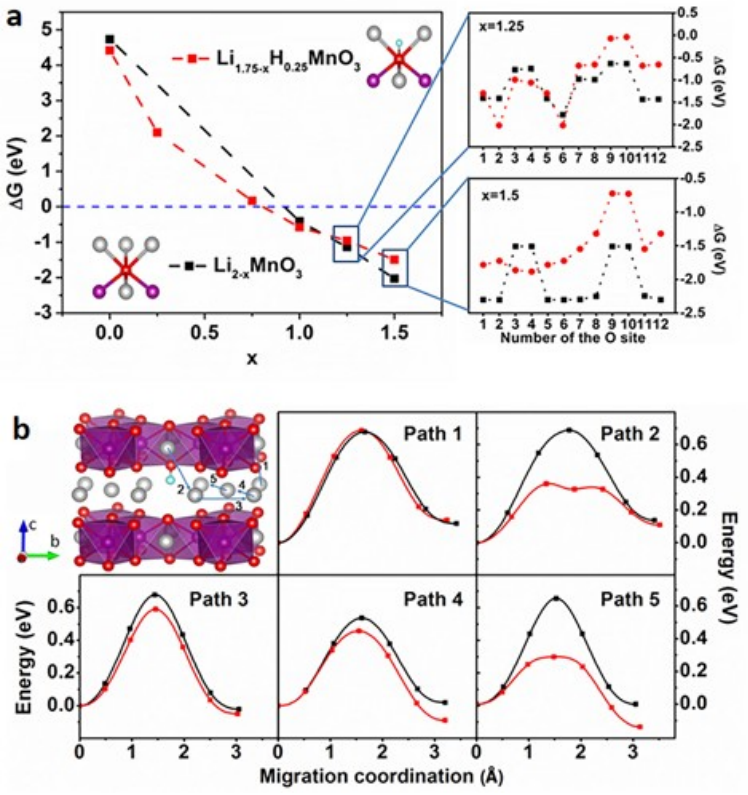

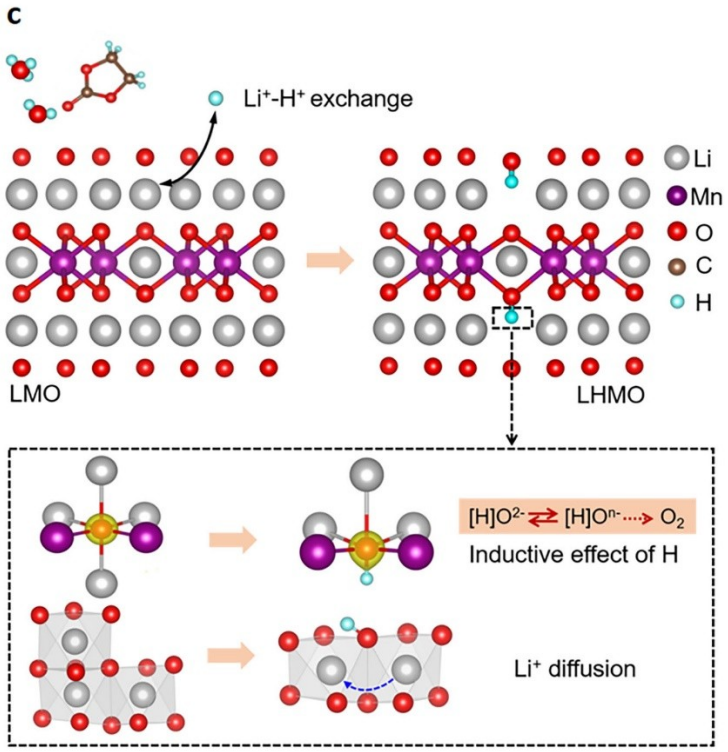

Figure 4. The intrinsic mechanism of protons insertion. (a) The Gibbs free energy for oxygen release reaction during delithiation process for $Li_{2-x}MnO_3$ and $Li_{1.75-x}H_{0.25}MnO_3$ (x=0, 0.25, 0.75, 1.0, 1.25, 1.5). **(b)** Schematic illustration of the possible Li^+ diffusion paths. The paths are shown by blue lines connecting two Li sites and labeled from 1 to 5. The migration barriers are compared in LMO (black) and LHMO (red). **(c)** Schematic illustration for reaction mechanism. The protons insert into layered structure via chemical/electrochemical treatment. During cycling, the oxygen activity could be modified with the inductive effect from the proton and effective Li^+ diffusion, leading to a controlled oxidation of the oxygen and reversible oxygen redox reactions.

In order to further understand the effect of protons on oxygen redox reaction, the DFT calculations were carried out with the model of LMO and $Li_{1.75}H_{0.25}MnO_3$ (LHMO) (**Figure 4**a, **4**b, **Figure S6**), in which the proton is at the site of (0.3799, 0.5000, 0.6008). From the calculated density of states (DOS) results, the band gap of DOS in LHMO decreases compared to that in pristine LMO, consistent with the lower beginning potential in LHMO based on both experimental and theoretical result (**Figure S11**). Unlike pristine LMO, which is well ordered and has only two environments for the oxygen atoms (i.e. O 4i and O 8j site), a variety of local oxygen environments exist in LHMO. The oxygen atoms are thus labeled from O1 to O12, according to the different distances between O and H atoms. The proton with high polarization nature forms O-H bounding with O10, which places the DOS for O10 relatively down in energy (**Figure S11**). The possibility of O_2 release at various delithiation stages was calculated by the Gibbs free energy (**Figure 4**a, **Figure S12**, **Note S2**). The value of ΔG is below zero at highly charged states, which means the lattice oxygen tends to release, this is consistent with the observation of oxygen gas at high level of delithiation[15,46,47]. However, after Li^+-H^+ exchange, even at high charged states (x=1.25, 1.5), the value of ΔG increases, which suggests it is more difficult for the oxygen to release from LHMO, especially for the oxygen atoms close to protons. This protonation effect is in perfect agreement with our mRIXS observations, which show a reversible evolution of the oxidized lattice oxygen feature with high discharge capacity.

Considering that the electrochemical process is dependent on both the charge compensation and Li^+ diffusion process, the behavior of Li^+ diffusion is exploited here**.** The results (**Figure 4**b, **Table S6**) show protons insertion facilitates the Li^+ diffusion via reducing the energy barrier for Li^+ hopping. Noticeably, the promoted Li^+ diffusion may also accelerate the reduction kinetics of peroxo-like species[48]. This additional benefit explains the experimental findings of the improved rate performance of LMO-acid (**Figure 2**c) and increased Li^+ diffusion coefficient (**Figure S13**).

CONCLUSION

In summary, a series experimental and theoretical study are performed towards the protonation effect on electrochemical performance of the representative LMO system. The special role that protons play on the electrochemical performance of LMO is schematically summarized in **Figure 4**c. Partial substitution with protons alters the oxygen activities through an effective inductive effect. Such a modified oxygen activity leads to outstanding initial cycle performance with greatly improved discharge capacity of 302 mAh g^{-1} and unprecedented Coulombic efficiency of 99.2%. The demonstrations and characterizations in this work not only reveal and explain the critical effect of protonation on electrochemistry involving oxygen redox reactions, more importantly, it paves a new way for the fundamental understanding on stabilizing oxygen redox reactions, which is critical for optimizing high-capacity cathode materials.

ASSOCIATED CONTENT

Supporting Information

Methods.

Figures for XRD patterns of the pristine and solution-treated LMO; SEM images; TGA data and TGA-MS data; The MS data and XRD patterns of the pristine and solution-treated LMO samples after TGA-MS test; Schematic representation of the optimized model; Schematic of LMO with protons insertion from BVS maps; Fitted ^{2}H MAS NMR spectra obtained at 50 kHz for deuterated LMO-acid sample; Electrochemical performance; The mapping of O K-edge mRIXS spectra for LMO; The DFT studies on the intrinsic mechanism of protons insertion; Convex hull of at different Li concentrations.; Nyquist plots of cells after initially discharged to 2.0 V.

Tables for the pH values of solutions during solution-treating process; The comparison on energy for LHMO with protons in different sites; Refinement results for the solution-treated and deuterated LMO; Refined crystallographic parameters; Electrochemical data in initial cycle; The calculated activation barriers for different Li^{+} diffusion paths.

Notes for the calculation of BVS maps; Calculation on Gibbs free energy for the oxygen evolution.

AUTHOR INFORMATION

Corresponding Author

* yyang@xmu.edu.cn

* wlyang@lbl.gov

Notes

The authors declare no competing financial interest.

ACKNOWLEDGMENT

This research was financially supported by National Natural Science Foundation of China (NNSFC, Grant No. 21233004, 21473148, 21621091, 21761132030), and National Key R&D Program of China (No. 2018YFB0905400, 2016YFB0901500). The authors thank M. Feng for experimental assistance, Dr. G. M. Zhong, G. R. Zheng for valuable discussion. The neutron experiments benefited from the SNS user facility, sponsored by the office of Basic Energy Sciences (BES), the Office of Science of the DOE. The authors thank Dr. Y. Chen and Dr. K. An from SNS for the technique support of neutron experiment. R.F. also wishes to acknowledge support from the National High Magnetic Field Lab (NHMFL) which is supported by the NSF Cooperative Agreement No. DMR-1644779 and the State of Florida. Soft X-ray spectroscopy uses the resource at the Advanced Light Source, which is a DOE Office of Science User Facility under contract no. DE-AC02-05CH11231. W.Y. and Ju.W. acknowledge the support from the Energy Biosciences Institute through the EBI-Shell program. Ju. W. acknowledge the support from graduate exchange program of Xiamen

University and double first-rate program in College of Chemistry and Chemical Engineering of Xiamen University. W.Y. would like to thank Prof. Y. Yao at UH for inspiring discussions on organic references.

REFERENCES

1. Hy, S.; Liu, H.; Zhang, M.; Qian, D.; Hwang, B.-J.; Meng, Y. S., Performance and Design Considerations for Lithium Excess Layered Oxide Positive Electrode Materials for Lithium Ion Batteries. *Energy Environ. Sci.* **2016,** *9*, 1931-1954.
2. Xia, Q.; Zhao, X.; Xu, M.; Ding, Z.; Liu, J.; Chen, L.; Ivey, D. G.; Wei, W., A Li-Rich Layered@Spinel@Carbon Heterostructured Cathode Material for High Capacity and High Rate Lithium-Ion Batteries Fabricated Via an in Situ Synchronous Carbonization-Reduction Method. *J. Mater. Chem. A* **2015,** *3*, 3995-4003.
3. Koga, H.; Croguennec, L.; Ménétrier, M.; Douhil, K.; Belin, S.; Bourgeois, L.; Suard, E.; Weill, F.; Delmas, C., Reversible Oxygen Participation to the Redox Processes Revealed for $Li_{1.20}Mn_{0.54}Co_{0.13}Ni_{0.13}O_2$. *J. Electrochem. Soc.* **2013,** *160*, A786-A792.
4. Zheng, J.; Myeong, S.; Cho, W.; Yan, P.; Xiao, J.; Wang, C.; Cho, J.; Zhang, J. G., Li-and Mn-Rich Cathode Materials: Challenges to Commercialization. *Adv. Energy Mater.* **2017,** *7*, 1601284.
5. Manthiram, A.; Knight, J. C.; Myung, S. T.; Oh, S. M.; Sun, Y. K., Nickel-Rich and Lithium-Rich Layered Oxide Cathodes: Progress and Perspectives. *Adv. Energy Mater.* **2016,** *6*, 1501010.
6. Li, B.; Xia, D., Anionic Redox in Rechargeable Lithium Batteries. *Adv. Mater.* **2017,** *29*, 1701054.
7. Denis, Y.; Yanagida, K.; Kato, Y.; Nakamura, H., Electrochemical Activities in Li_2MnO_3. *J. Electrochem. Soc.* **2009,** *156*, A417-A424.
8. Yu, F.-D.; Que, L.-F.; Wang, Z.-B.; Xue, Y.; Zhang, Y.; Liu, B.-S.; Gu, D.-M., Controllable Synthesis of Hierarchical Ball-in-Ball Hollow Microspheres for a High Performance Layered Li-Rich Oxide Cathode Material. *J. Mater. Chem. A* **2017,** *5*, 9365-9376.
9. Singer, A.; Zhang, M.; Hy, S.; Cela, D.; Fang, C.; Wynn, T. A.; Qiu, B.; Xia, Y.; Liu, Z.; Ulvestad, A.; Hua, N.; Wingert, J.; Liu, H.; Sprung, M.; Zozulya, A. V.; Maxey, E.; Harder, R.; Meng, Y. S.; Shpyrko, O. G., Nucleation of Dislocations and Their Dynamics in Layered Oxide Cathode Materials During Battery Charging. *Nat. Energy* **2018,** *3*, 641-647.
10. Croy, J. R.; Balasubramanian, M.; Gallagher, K. G.; Burrell, A. K., Review of the US Department of Energy's "Deep Dive" Effort to Understand Voltage Fade in Li-and Mn-Rich Cathodes. *Acc. Chem. Res.* **2015,** *48*, 2813-2821.
11. Sun, G.; Yu, F.-D.; Que, L.-F.; Deng, L.; Wang, M.-J.; Jiang, Y.-S.; Shao, G.;

Wang, Z.-B., Local Electronic Structure Modulation Enhances Operating Voltage in Li-Rich Cathodes. *Nano Energy* **2019,** *66*, 104102.
12. Yang, W., Oxygen Release and Oxygen Redox. *Nat. Energy* **2018,** *3*, 619-620.
13. Hu, E.; Yu, X.; Lin, R.; Bi, X.; Lu, J.; Bak, S.; Nam, K.-W.; Xin, H. L.; Jaye, C.; Fischer, D. A., Evolution of Redox Couples in Li-and Mn-Rich Cathode Materials and Mitigation of Voltage Fade by Reducing Oxygen Release. *Nat. Energy* **2018,** *3*, 690-698.
14. Li, N.; Hwang, S.; Sun, M.; Fu, Y.; Battaglia, V. S.; Su, D.; Tong, W., Unraveling the Voltage Decay Phenomenon in Li-Rich Layered Oxide Cathode of No Oxygen Activity. *Adv. Energy Mater.* **2019,** *9*, 1902258.
15. Luo, K.; Roberts, M. R.; Hao, R.; Guerrini, N.; Pickup, D. M.; Liu, Y.-S.; Edström, K.; Guo, J.; Chadwick, A. V.; Duda, L. C., Charge-Compensation in 3d-Transition-Metal-Oxide Intercalation Cathodes through the Generation of Localized Electron Holes on Oxygen. *Nat. Chem.* **2016,** *8*, 684-691.
16. Armstrong, A. R.; Holzapfel, M.; Novák, P.; Johnson, C. S.; Kang, S.-H.; Thackeray, M. M.; Bruce, P. G., Demonstrating Oxygen Loss and Associated Structural Reorganization in the Lithium Battery Cathode $Li[Ni_{0.2}Li_{0.2}Mn_{0.6}]O_2$. *J. Am. Chem. Soc.* **2006,** *128*, 8694-8698.
17. Dai, K.; Wu, J.; Zhuo, Z.; Li, Q.; Sallis, S.; Mao, J.; Ai, G.; Sun, C.; Li, Z.; Gent, W. E., High Reversibility of Lattice Oxygen Redox Quantified by Direct Bulk Probes of Both Anionic and Cationic Redox Reactions. *Joule* **2019,** *3*, 518-541.
18. Padhi, A. K.; Nanjundaswamy, K. S.; Goodenough, J. B., Phospho-Olivines as Positive-Electrode Materials for Rechargeable Lithium Batteries. *J. Electrochem. Soc.* **1997,** *144*, 1188-1194.
19. Liu, X.; Wang, Y. J.; Barbiellini, B.; Hafiz, H.; Basak, S.; Liu, J.; Richardson, T.; Shu, G.; Chou, F.; Weng, T. C.; Nordlund, D.; Sokaras, D.; Moritz, B.; Devereaux, T. P.; Qiao, R.; Chuang, Y. D.; Bansil, A.; Hussain, Z.; Yang, W., Why $LiFePO_4$ Is a Safe Battery Electrode: Coulomb Repulsion Induced Electron-State Reshuffling Upon Lithiation. *Phys. Chem. Chem. Phys.* **2015,** *17*, 26369- 26377.
20. Zhou, F.; Kang, K.; Maxisch, T.; Ceder, G.; Morgan, D., The Electronic Structure and Band Gap of $LiFePO_4$ and $LiMnPO_4$. *Solid State Commun.* **2004,** *132*, 181-186.
21. Pohl, R.; Antognini, A.; Nez, F.; Amaro, F. D.; Biraben, F.; Cardoso, J. M.; Covita, D. S.; Dax, A.; Dhawan, S.; Fernandes, L. M., The Size of the Proton. *Nature* **2010,** *466*, 213-216.
22. Perez, A. J.; Beer, R.; Lin, Z.; Salager, E.; Taberna, P. L.; Abakumov, A. M.; Simon, P.; Tarascon, J. M., Proton Ion Exchange Reaction in Li_3IrO_4: A Way to New $H_{3+x}IrO_4$ Phases Electrochemically Active in Both Aqueous and Nonaqueous Electrolytes. *Adv. Energy Mater.* **2018,** *8*, 1702855.
23. Paik, Y.; Grey, C. P.; Johnson, C. S.; Kim, J.-S.; Thackeray, M. M., Lithium and Deuterium Nmr Studies of Acid-Leached Layered Lithium Manganese Oxides. *Chem. Mater.* **2002,** *14*, 5109-5115.

24. Robertson, A. D.; Bruce, P. G., Mechanism of Electrochemical Activity in Li_2MnO_3. *Chem. Mater.* **2003,** *15*, 1984-1992.
25. Venkatraman, S.; Manthiram, A., Investigation of the Possible Incorporation of Protons into Oxide Cathodes During Chemical Delithiation. *J. Solid State Chem.* **2004,** *177*, 4244-4250.
26. Tang, W.; Kanoh, H.; Yang, X.; Ooi, K., Preparation of Plate-Form Manganese Oxide by Selective Lithium Extraction from Monoclinic Li_2MnO_3 under Hydrothermal Conditions. *Chem. Mater.* **2000,** *12*, 3271-3279.
27. Kang, S.-H.; Johnson, C.; Vaughey, J.; Amine, K.; Thackeray, M., The Effects of Acid Treatment on the Electrochemical Properties of $0.5Li_2MnO_3 \bullet 0.5LiNi_{0.44}Co_{0.25}Mn_{0.31}O_2$ Electrodes in Lithium Cells. *J. Electrochem. Soc.* **2006,** *153*, A1186-A1192.
28. Choi, J.; Alvarez, E.; Arunkumar, T.; Manthiram, A., Proton Insertion into Oxide Cathodes During Chemical Delithiation. *Electrochemical solid-state letters* **2006,** *9*, A241-A244.
29. Ammundsen, B.; Jones, D. J.; Rozière, J.; Berg, H.; Tellgren, R.; Thomas, J. O., Ion Exchange in Manganese Dioxide Spinel: Proton, Deuteron, and Lithium Sites Determined from Neutron Powder Diffraction Data. *Chem. Mater.* **1998,** *10*, 1680-1687.
30. Galven, C.; Dittmer, J.; Suard, E.; Le Berre, F. o.; Crosnier-Lopez, M.-P., Instability of Lithium Garnets against Moisture. Structural Characterization and Dynamics of $Li_{7-X}H_xLa_3Sn_2O_{12}$ and $Li_{5-X}H_xLa_3Nb_2O_{12}$. *Chem. Mater.* **2012,** *24*, 3335-3345.
31. Orera, A.; Larraz, G.; Rodríguez-Velamazán, J. A.; Campo, J.; Sanjuán, M. L., Influence of Li^+ and H^+ Distribution on the Crystal Structure of $Li_{7-x}H_xLa_3Zr_2O_{12}$ ($0 \leq X \leq 5$) Garnets. *Inorg. Chem.* **2016,** *55*, 1324-1332.
32. Lee, S.; Choi, S.; Kim, J.; Sim, H.; Won, C.; Lee, S.; Kim, S. A.; Hur, N.; Park, J.-G., Antiferromagnetic Ordering in Li_2MnO_3 Single Crystals with a Two-Dimensional Honeycomb Lattice. *J. Phys.: Condens. Matter* **2012,** *24*, 456004.
33. Dogan, F.; Croy, J. R.; Balasubramanian, M.; Slater, M. D.; Iddir, H.; Johnson, C. S.; Vaughey, J. T.; Key, B., Solid State Nmr Studies of Li_2MnO_3 and Li-Rich Cathode Materials: Proton Insertion, Local Structure, and Voltage Fade. *J. Electrochem. Soc.* **2015,** *162*, A235-A243.
34. Paik, Y.; Osegovic, J. P.; Wang, F.; Bowden, W.; Grey, C. P., ^2H MAS NMR Studies of the Manganese Dioxide Tunnel Structures and Hydroxides Used as Cathode Materials in Primary Batteries. *J. Am. Chem. Soc.* **2001,** *123*, 9367-9377.
35. McCalla, E.; Abakumov, A. M.; Saubanère, M.; Foix, D.; Berg, E. J.; Rousse, G.; Doublet, M.-L.; Gonbeau, D.; Novák, P.; Van Tendeloo, G. J. S., Visualization of O-O Peroxo-Like Dimers in High-Capacity Layered Oxides for Li-Ion Batteries. **2015,** *350*, 1516-1521.
36. Yoon, W.-S.; Kim, N.; Yang, X.-Q.; McBreen, J.; Grey, C. P., ^6Li MAS NMR and in Situ X-Ray Studies of Lithium Nickel Manganese Oxides. *J. Power Sources* **2003,** *119*, 649-653.

37. Dai, K.; Wu, J.; Zhuo, Z.; Li, Q.; Sallis, S.; Mao, J.; Ai, G.; Sun, C.; Li, Z.; Gent, W. E.; Chueh, W. C.; Chuang, Y.-d.; Zeng, R.; Shen, Z.-x.; Pan, F.; Yan, S.; Piper, L. F. J.; Hussain, Z.; Liu, G.; Yang, W., High Reversibility of Lattice Oxygen Redox Quantified by Direct Bulk Probes of Both Anionic and Cationic Redox Reactions. *Joule* **2019,** *3*, 518-541.
38. Shimoda, K.; Oishi, M.; Matsunaga, T.; Murakami, M.; Yamanaka, K.; Arai, H.; Ukyo, Y.; Uchimoto, Y.; Ohta, T.; Matsubara, E.; Ogumi, Z., Direct Observation of Layered-to-Spinel Phase Transformation in Li_2MnO_3 and the Spinel Structure Stabilised after the Activation Process. *J. Mater. Chem. A* **2017,** *5*, 6695-6707.
39. Yang, W.; Devereaux, T. P., Anionic and Cationic Redox and Interfaces in Batteries: Advances from Soft X-Ray Absorption Spectroscopy to Resonant Inelastic Scattering. *J. Power Sources* **2018,** *389*, 188-197.
40. Gent, W. E.; Lim, K.; Liang, Y.; Li, Q.; Barnes, T.; Ahn, S.-J.; Stone, K. H.; McIntire, M.; Hong, J.; Song, J. H., Coupling between Oxygen Redox and Cation Migration Explains Unusual Electrochemistry in Lithium-Rich Layered Oxides. *Nat. Commun.* **2017,** *8*, 2091.
41. Zhuo, Z.; Pemmaraju, C. D.; Vinson, J.; Jia, C.; Moritz, B.; Lee, I.; Sallies, S.; Li, Q.; Wu, J.; Dai, K., Spectroscopic Signature of Oxidized Oxygen States in Peroxides. *J. Phys. Chem. Lett.* **2018,** *9*, 6378-6384.
42. Qiao, R.; Li, Q.; Zhuo, Z.; Sallis, S.; Fuchs, O.; Blum, M.; Weinhardt, L.; Heske, C.; Pepper, J.; Jones, M., High-Efficiency in Situ Resonant Inelastic X-Ray Scattering (iRIXS) Endstation at the Advanced Light Source. *Rev. Sci. Instrum.* **2017,** *88*, 033106.
43. Xu, J.; Sun, M.; Qiao, R.; Renfrew, S. E.; Ma, L.; Wu, T.; Hwang, S.; Nordlund, D.; Su, D.; Amine, K., Elucidating Anionic Oxygen Activity in Lithium-Rich Layered Oxides. *Nat. Commun.* **2018,** *9*, 947.
44. Hauge, J. G., Glucose Dehydrogenase of Bacterium Anitratum: An Enzyme with a Novel Prosthetic Group. *J. Biol. Chem.* **1964,** *239*, 3630-3639.
45. Liang, Y.; Jing, Y.; Gheytani, S.; Lee, K.-Y.; Liu, P.; Facchetti, A.; Yao, Y., Universal Quinone Electrodes for Long Cycle Life Aqueous Rechargeable Batteries. *Nat. Mater.* **2017,** *16*, 841-848.
46. Maitra, U.; House, R. A.; Somerville, J. W.; Tapia-Ruiz, N.; Lozano, J. G.; Guerrini, N.; Hao, R.; Luo, K.; Jin, L.; Pérez-Osorio, M. A., Oxygen Redox Chemistry without Excess Alkali-Metal Ions in $Na_{2/3}[Mg_{0.28}Mn_{0.72}]O_2$. *Nat. Chem.* **2018,** *10*, 288-295.
47. Strehle, B.; Kleiner, K.; Jung, R.; Chesneau, F.; Mendez, M.; Gasteiger, H. A.; Piana, M., The Role of Oxygen Release from Li-and Mn-Rich Layered Oxides During the First Cycles Investigated by on-Line Electrochemical Mass Spectrometry. *J. Electrochem. Soc.* **2017,** *164*, A400-A406.
48. Assat, G.; Delacourt, C.; Dalla Corte, D. A.; Tarascon, J.-M., Practical Assessment of Anionic Redox in Li-Rich Layered Oxide Cathodes: A Mixed Blessing for High Energy Li-Ion Batteries. *J. Electrochem. Soc.* **2016,** *163*, A2965-A2976.